DESIGN OPTIMIZATION OF VERTICAL NEEDLE GEOMETRY FOR BUMP WAFER-LEVEL PROBING

Te-Ching Hsiao[1], Shyh-Chour Huang[1] and Hao-Yuan Chang[2]
[1]*Department of Mechanical Engineering, National Kaohsiung University of Applied Sciences, Kaohsiung, Taiwan, R.O.C.*
[2]*Advanced Semiconductor Engineering, Inc., Nantze Export Processing Zone, Kaohsiung, Taiwan, R.O.C.*
E-mail: jacadikimo@yahoo.com.tw

Received November 2016, Accepted February 2017
No. 16-CSME-139, E.I.C. Accession 4025

ABSTRACT

The purpose of this paper is mainly to develop a method to use the Taguchi method with the L_{18} $(2^1 \times 3^7)$ orthogonal array to obtain an optimal geometrical design of the vertical probing needle and base on various criteria to minimize the stress on the probing needle during wafer-level probing test. Furthermore, importance of the factors on the probing mark area ratio was also ranked. The results shows that as probe length, offset, and lower die gap increase, stress on the probing decrease. On the contrary, vertical probe bends decrease, stress on the probe increase. Furthermore, the body of vertical probe with rectangle cross-section is better than square and circular sharp.

Keywords: wafer probing; Taguchi method; probing mark area ratio.

OPTIMISATION DE LA CONCEPTION DE LA GÉOMÉRIE VERTICALE DE L'AIGUILLE DE SONDE SUR LE PROBE DE PLAQUETTES

RÉSUMÉ

Le but principal de l'étude est de développer une façon d'utiliser la méthode Taguchi avec la formule orthogonale $(2^1 \times 3^7)$ pour obtenir la conception géométrique optimale de l'aiguille verticale du probe, et en se basant sur différents critères, réduire la tension sur l'aiguille du probe pendant le test sur plaquettes. De plus, l'importance de ces facteurs sur le taux de marques dans la zone du probe est également considérée. Les résultats démontrent que, plus grande est la longueur du probe, le décalage et l'augmentation de l'intervalle de la matrice inférieure, plus la tension sur le probe diminue. À l'inverse, quand il y diminution de la courbe de la sonde verticale, la tension sur le probe augmente. Le corps du probe vertical avec une section transversale rectangulaire est préférable à la coupe carré et circulaire.

Mots-clés : test du probe de plaquettes ; méthode Taguchi ; taux de marques sur la zone du probe.

1. INTRODUCTION

The vertical probe card called 'Cobra' is a reliable solution with the ability to address wafer testing challenges and to satisfy some probing requirements, such as multiple IC's and area array solder bump probing as shown in Fig. 1. In the 1970s, IBM developed the Cobra probe card to probe C4 (controlled collapse chip connect) bumps. There are several advantages of the vertical probing technology which are as follows: (1) it can be applied to area array bumps and probe marks are more uniform than those formed by using the cantilever probe card [1, 2]; (2) through the deflection of the vertical probe, the contact force on the bump sphere is almost uniform; (3) it can be applied to high speed wafer-level testing which has high resolution [3, 4]; (4) it can further be utilized for the probing of copper pillars with solder caps [5–8]; (5) other advantages include durability, interchangeability, single probe replacement, high probe density and it overcomes the mechanical and spatial restrictions of the conventional cantilever probe card [3, 4]. The vertical probe card is able to perform high-speed probing of densely packed solder bump arrays for logic devices. Moreover, the vertical probe card provides a variety of application-specific design options, including wired space transformers, Multi-Layer Ceramic (MLC), Multi-Layer Organic (MLO), and Modular Space Transformer (MST) [9, 10].

Although many studies have been done before on bump probing and Al (aluminum) pad probing with cantilever probe card, less research has been reports on the topic of design optimization of vertical needle geometry. An excessive probing scrub not only damages the solder bump but also destabilizes the electrical contact of needles after repeated probing due to gradual accumulation of coplanarity variation on the probes [11, 12]. Therefore, It is necessary to establish the optimized method to enhance the probe lifespan and the test yield, since the bump height variation and probe mark area ratio influence the quality of bump wafer sorting and further impact the reliability of the flip chip assembly process. In other words, the establishment of standard selection of feasible needle geometry rules can satisfy probing requirements of various up-to-date devices [13]. In addition, it is effective to control the appropriate bump height and probe mark quality to enhance the reliability of the chip package and to avoid the solder bump damage and cold joint issue.

In this paper, the Taguchi method with the $L_{18}(2^1 \times 3^7)$ orthogonal array was employed to optimize the vertical needle geometry during the wafer-level probing test of a memory device. Effects of different geometrical factors of the probing needle, including probe mid-length, offset, cross-section of body(mid-sharp), the radius of bends and lower die gap were evaluated.

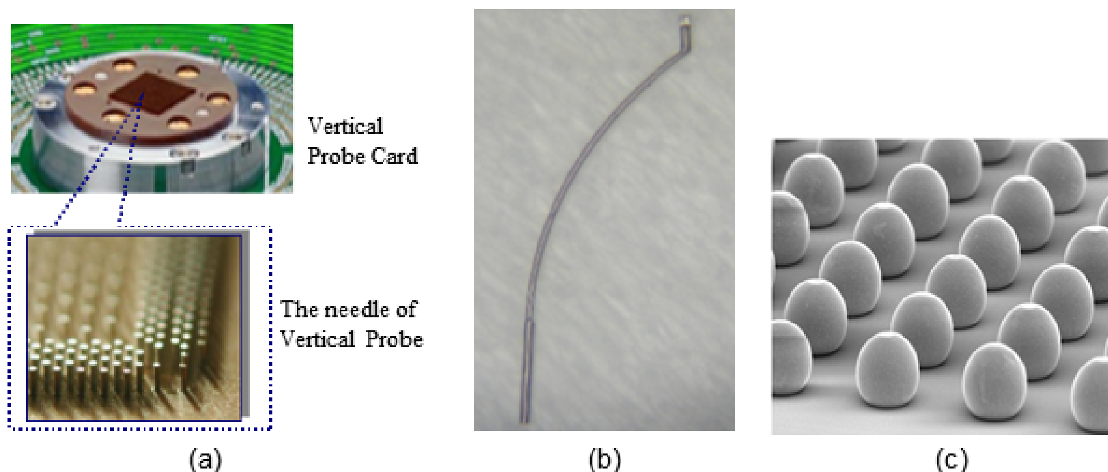

Fig. 1. Vertical Probe care and the array solder bump on chip: (a) the top view of vertical probe card; (b) the side view of vertical probe; (c) the array solder bump on chip.

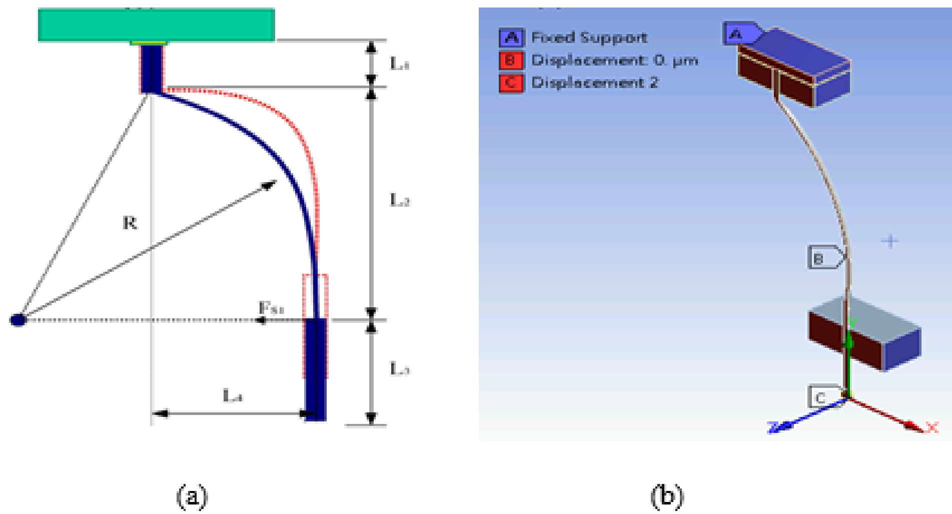

Fig. 2. (a) Vertical probe geometry and (b) finite element model and the boundary condition of the vertical probe and the solder bump.

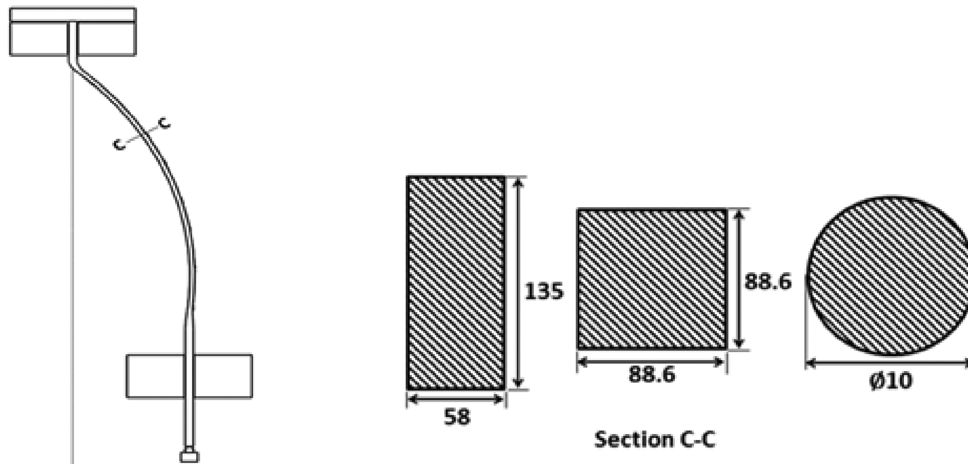

Fig. 3. The different shape of the cross sections of vertical probe (unit: μm).

2. FINITE-ELEMENT MODELING

In this section, the finite element analysis and ANSYS finite element code was used to simulate the contact behavior between the vertical probe and the solder bump. To ensure that the needle moves on the X-Y plane and it has the vertical displacement on the X-Z plane, as shown in Fig. 2. Table 1 shows the each dimensions of vertical probe. The upper and lower die, which are used to constrained all of degree of freedom of the vertical probe. The solder bump moves up along to a specific trajectory and then contacts with the needle tip.

The material of the vertical probe is Paliney 7 (P7) with various probe mid-sharp. In terms of the finite-element simulations, the bump materialof Eutectic (63Sn/37Pb) is used in the simulation. The probe diameter is 4 mils ($\sim$ 100 μm) and we consider different shape of the cross section in curved part of vertical probe as shown in Fig. 3 and the heights of the solder bump and diameter are 85 and 105 μm, respectively as

Table 1. Dimensions of vertical probe (unit: μm).

Tip Diameter	Probe Length	Tip Length	Mid-Length	Offset	Head Length	Radius
(D)	(L_p)	(L_3)	(L_2)	(L_4)	(L_1)	(R)
100	6100	1800	3700	1200	600	5800

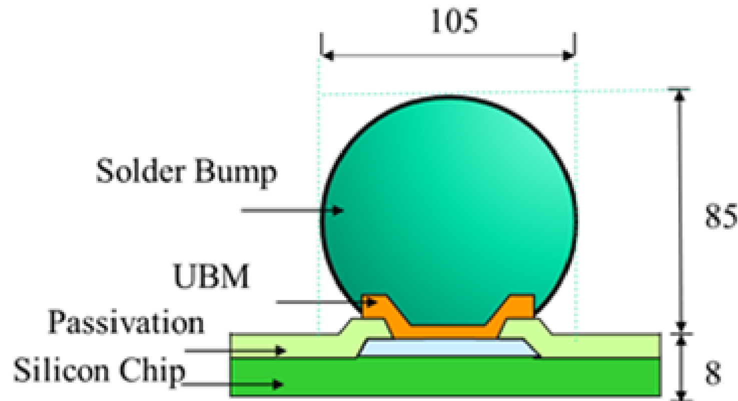

Fig. 4. The solder bump structures (unit: μm).

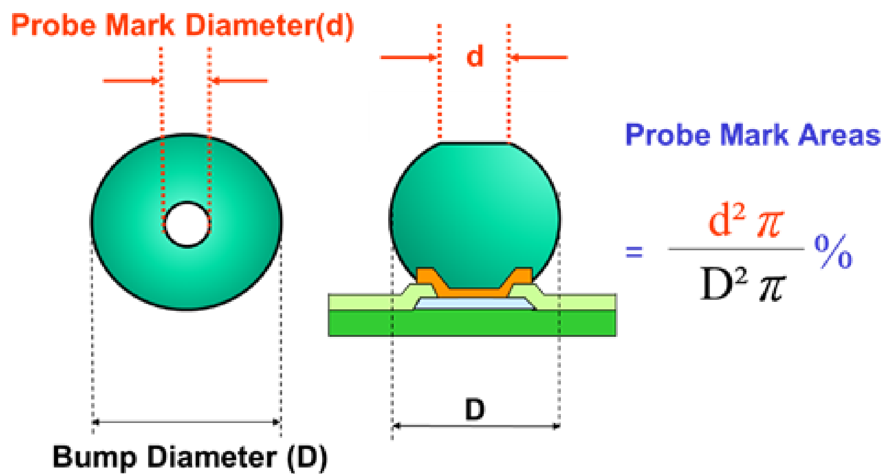

Fig. 5. The measurement method of probe mark area ratio (from the top view of solder bump).

shown in Fig. 4. In addition, Fig. 5 shows that the method of probe mark area ratio measurement. Figure 6 shows the top view of solder bump and the probe mark area ratio enlarge with overdrive (OD) increase.

The mesh is made by the following elements Hex 20. Besides, the stress of needle and probe mark area ratio can be convergence as the mesh sizes are set to 5 μm in the solder bump and 20 μm in the needle. In addition, convergence can be verified graphically. Figure 5 shows the plots of the convergence from the stress of needle and probe mark area ratio. In this paper, the response of the solder bump is described using the linear elastic, perfectly plastic stress-strain model. Specifically, the solder bump is modeled using 3864 solid elements and the needle is modeled with 5457 shell elements. The needle is referred to as a contact surface and the solder bump surface is as the target surface.

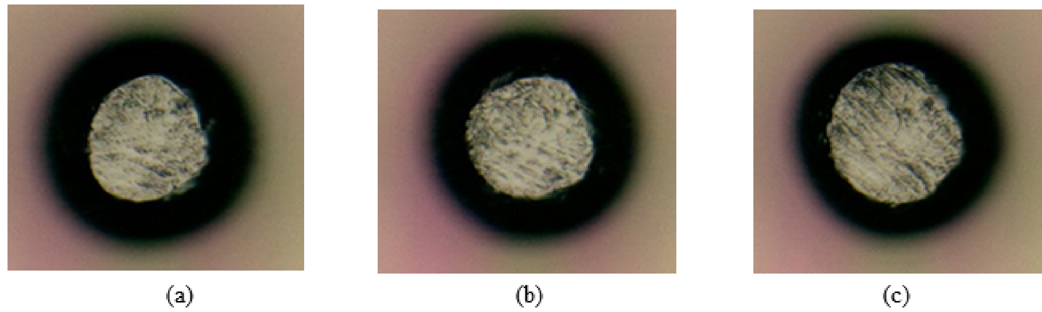

Fig. 6. Probe mark top view in solder bump on overdrive (OD) are (a) 75 µm; (b) 100 µm; (c) 125 µm.

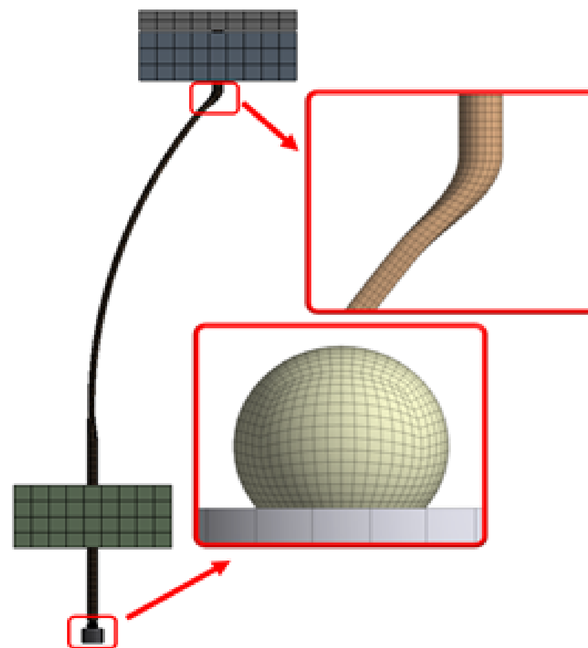

Fig. 7. Finite-Element model meshing and geometry of vertical probe.

Furthermore, the model meshing is shown in Fig. 7 and stress distribution of the head length is shown in Fig. 8. It is observed that the maximum effective stress is located in the elements which close to the top of probe mid-length which is a flexible spring and absorb the energy. It leads to stress values are greater than the yield stress and the tensile stress of the bump 25 MPa. Besides, it has further indicated that the maximum von Mises stresses. Overdrive 75, 100, 125 and 150 µm are 483.85, 579.14, 756.06 and 912.8 MPa, respectively as shown in Fig. 9.

It also demonstrates that the stress distributions in the bump is not uniform, since the opening of through holes, which have the tolerance about 10–20 µm through the lower and upper dies, influence the vertical moving of the vertical needle and not completely vertical contact with the solder bump. Figure 10 shows that the resultant force F is a single vertical force to act on the solder bump in the beginning. When the solder bump moving up, the resultant force F' can be divided to two perpendicular forces, and the x-component of the resultant Fx' makes the scrub on the solder bump.

Moreover, to validate the simulation model, the contact force and probe mark area ratio obtained from the finite element analysis as were good consistence with the probe mark area ratio obtained from the experi-

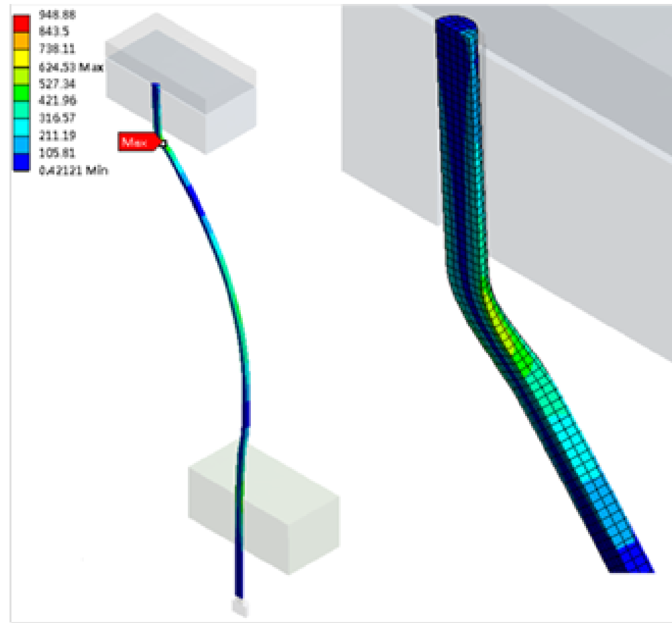

Fig. 8. The stress distribution of the head length of vertical probing needle.

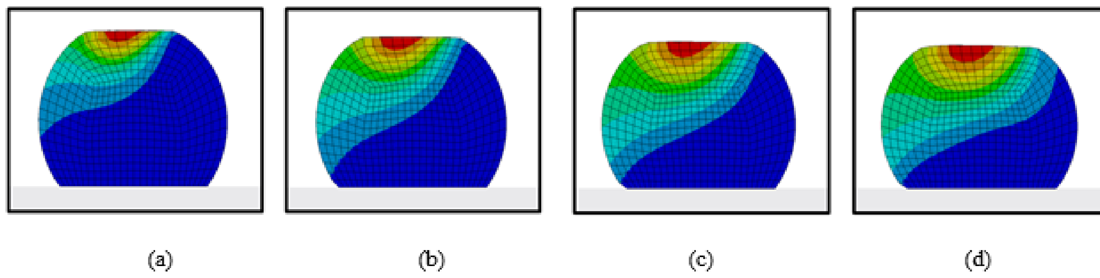

Fig. 9. Stress distribution of the solder bump (a) OD = 75 μm; (b) OD = 100 μm; (c) OD = 125 μm; (d) OD = 150 μm.

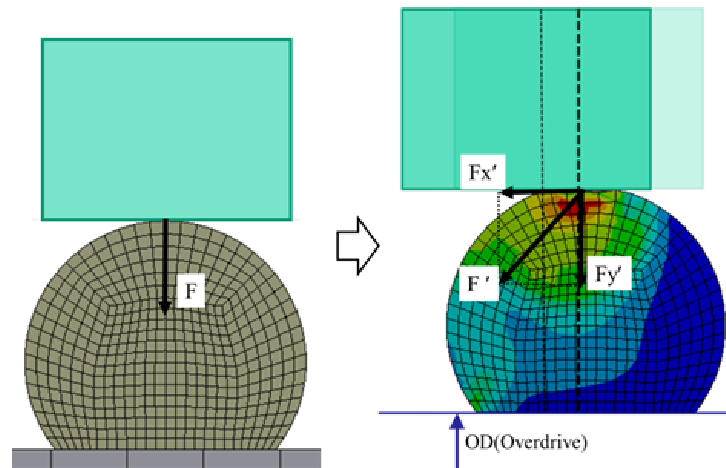

Fig. 10. Components of contact force.

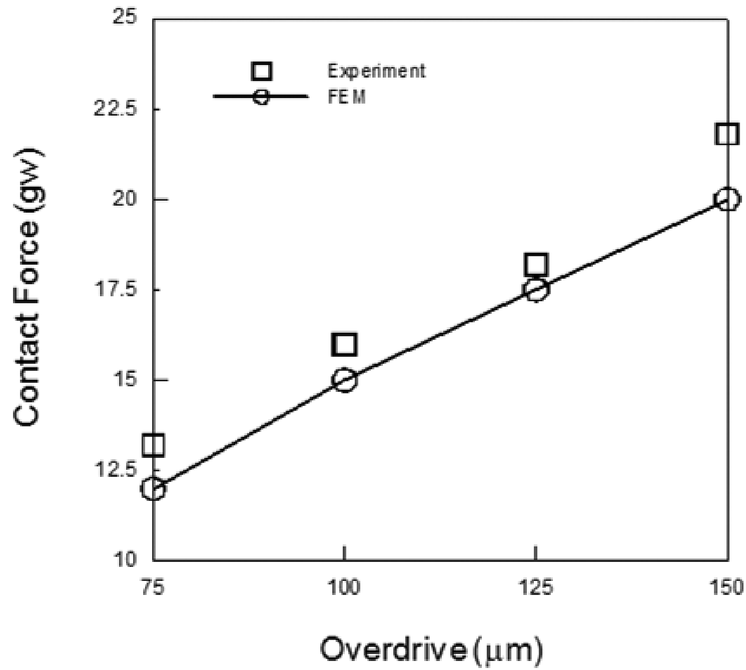

Fig. 11. Relationship between the contact force and the overdrive.

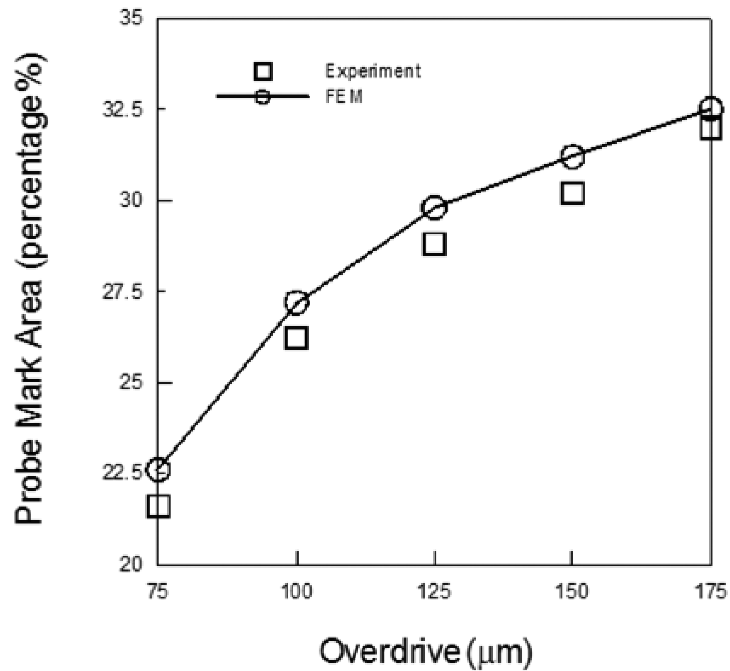

Fig. 12. Relationship between the probe mark area ratio and the overdrive.

mental probe mark area ratio as shown in Figs. 11 and 12. Table 2 shows the material properties of bump and probe using for analysis. From Tables 3 and 4, it can be seen that the discrepancy in the contact force is less than 13.4% and probe mark area ratio is less than 6.1%.

Table 2. Material properties of bump and probe [14–17].

Component	Material	Young's Modulus (GPa)	Poisson's Ratio	Yield Stress (MPa)	Tangent Modulus (GPa)
Solder Bump	63Sn/37Pb	32	0.35	25	145
Vertical Needle	P7	121	0.33	930	1767
Upper/Lower Die	Ceramic	200	0.23	–	–
Wafer	Silicon	130	0.28	–	–

Table 3. Comparison of experimental and simulation contact force with various overdrives.

Overdrive (μm)	Simulation (gw)	Experiment (gw)	Discrepancy (%)	von Mises stress (MPa) of Simulation
50	9.0	8.0	13.4	405.1
75	11.7	11.9	1.3	533.3
100	14.5	15.2	4.2	730.9
125	17.0	18.3	7.5	921.8
150	19.9	20.6	3.4	1103.2

Table 4. Comparison of experimental and simulation probe mark area ratio with various overdrives.

Overdrive (μm)	Simulation (%)	Experiment (%)	Discrepancy (%)
50	19.8	20.4	2.9
75	26.9	28.5	5.6
100	28.5	30.1	5.5
125	31.2	33.1	6.1
150	34.3	36.2	5.2

The consistence between the simulation and experimental results demonstrates the reliability of the finite element model. From simulation results, it has been figured out that the opening of through holes of the lower and upper dies will influence the moving of the vertical needle. This leads to the stress distribution inside the solder bump is not uniform.

3. OPTIMIZATION

The optimal design of the needle geometry is always an interesting problem and probing mark area ratio is an important index for wafer level probing. In the paper, application of Taguchi method to the optimization of bumping wafer probing and the scrub length was therefore chosen in this work as the quality factor. The Taguchi method applies fractional factorial experimental designs, called orthogonal arrays, to reduce the number of experiments and meanwhile obtaining statistically meaningful results. Probing parameters with the optimal probing mark area ratio are determined and verified. The goal of the Taguchi method is to find out the optimal and robust product or process characteristic that has a minimized sensitivity to noise. In this paper, by referring to [8, 9], the five selected control factors concerning the geometry of the probing needle and their levels are listed in Table 5. These control factors include (A) mid-length of probe (L_2), (B) offset (L_4), (C) mid-sharp, (D) radius (R), and (E) lower die gap. All control factors have three levels and underlined levels in the table represent original geometrical design parameters of the needle. The levels were selected within a reasonable design range of an actual product. According to the numbers of control factors and their levels listed in Table 5, the orthogonal array was employed in the main experiment to

Table 5. Control factors and levels (unit: μm).

Factor	Description	Level 1	Level 2	Level 3
hline A	mid- length (L_2)	3300	3700	4100
B	offset (L_4)	1000	1200	1400
C	mid-sharp	square	rectangle	circle
D	radius (R)	4300	4700	5100
E	Lower die gap	2.5	7.5	5

Table 6. The experimental results and S/N ratios of main experiment.

	Factors and levels					Y (probe mark	S/N
Experiment	A	B	C	D	E	ration) (%)	
hline 1	1	1	1	1	1	37.51	–31.48
2	1	2	2	2	2	24.18	–27.67
3	1	3	3	3	3	35.21	–30.93
4	2	1	1	2	2	25.00	–27.96
5	2	2	2	3	3	19.84	–25.95
6	2	3	3	1	1	24.20	–27.68
7	3	1	2	1	3	12.88	–22.20
8	3	2	3	2	1	24.56	–27.81
9	3	3	1	3	2	18.79	–25.48
10	1	1	3	3	2	33.49	–30.50
11	1	2	1	1	3	30.06	–29.56
12	1	3	2	2	1	28.54	–29.11
13	2	1	2	3	1	27.88	–28.90
14	2	2	3	1	2	23.13	–27.28
15	2	3	1	2	3	26.40	–28.43
16	3	1	3	2	3	23.30	–27.35
17	3	2	1	3	1	25.90	–28.27
18	3	3	2	1	2	11.00	–20.83
					Average	25.10	–27.63

Table 7. Response and ranks of S/N ratio of control factors.

	A	B	C	D	E
Level1	–29.88	–28.07	–28.53	–26.51	–28.87
Level2	–27.70	–27.76	–25.78	–28.05	–26.62
Level3	–25.32	–27.08	–28.59	–28.34	–27.40
Effect	4.56	0.99	2.81	1.83	2.25
Rank	1	5	2	4	3

minimize. The smaller-the signal-to-noise ratio (S/N), defined as

$$\mathrm{S/N}_{SB} = -10\log_{10}\frac{\sum_{i=1}^{n} y_i^2}{n} = -10\log_{10}(\bar{y}^2 + S_n^2) \quad (1)$$

where y is the measurement data (probe mark area ratio), n is the number of measurements, and S_n is standard deviation.

Since a numerical analysis cannot have data variations or experimental errors. Therefore, the main experiment is aimed at obtaining the optimal design. For the main experiment, the $L_{18}(2^1 \times 3^7)$ orthogonal array was implemented and the data were presented in Table 6. Table 7 and Fig. 13 show responses of control

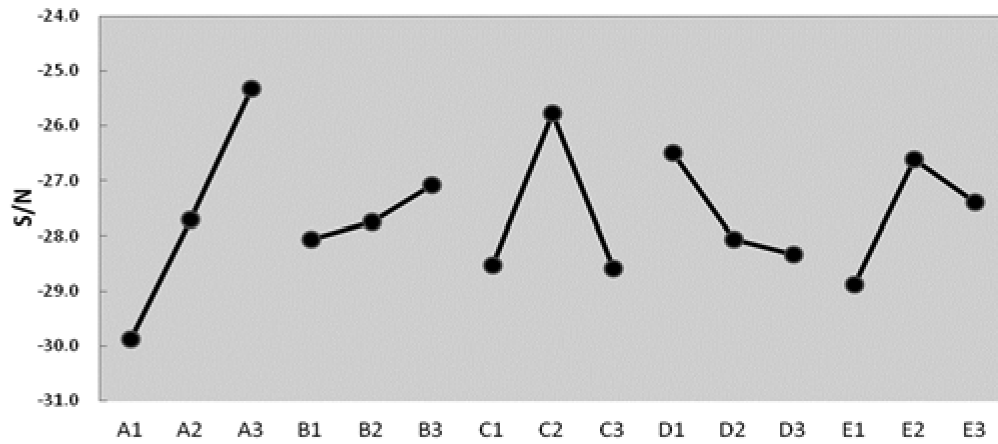

Fig. 13. Control factor response diagram of S/N.

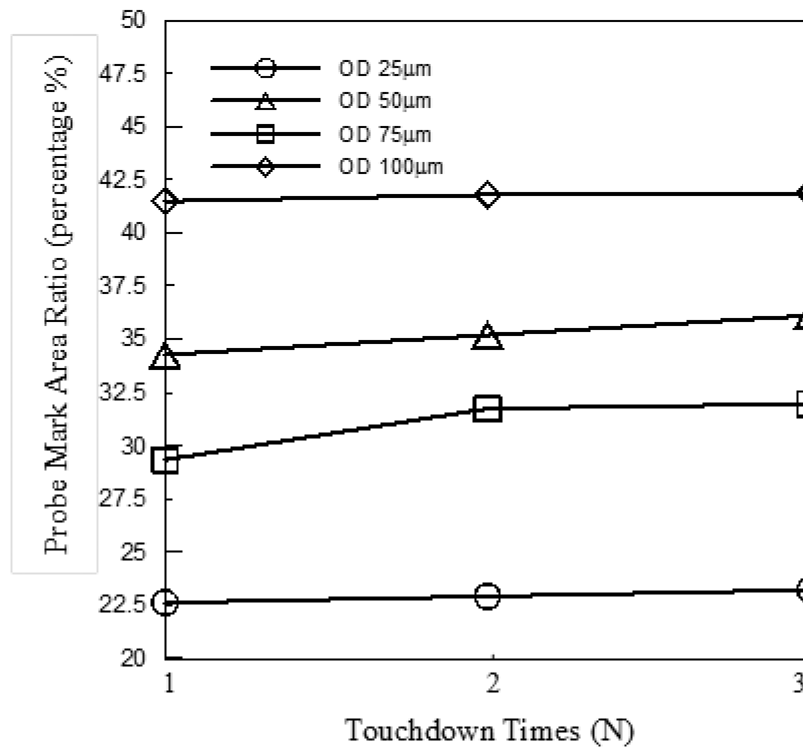

Fig. 14. Relationship between the probe mark area ratio and the touchdown times (N).

Table 8. Confirmation of the design optimization and original state

	A	B	C	D	E	S	S/N
Original	2	2	2	3	3	0.15	–25.95
Optimal	3	3	2	1	2	0.50	–20.83

factors calculated from the results presented in Table 6. In the table, the response for level of factor is defined as the average of factor at level. The effect denotes the difference between maximum and minimum

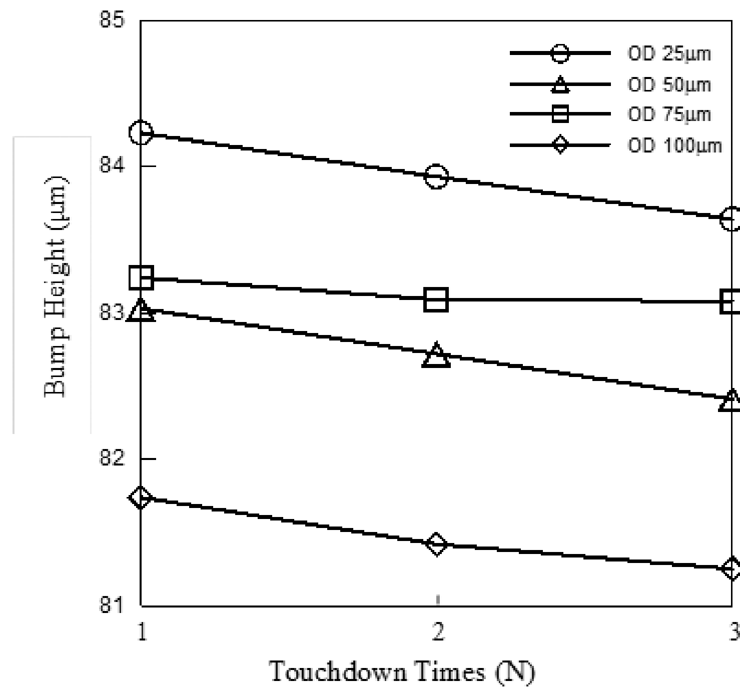

Fig. 15. Relationship between the bump height and the touchdown times (N).

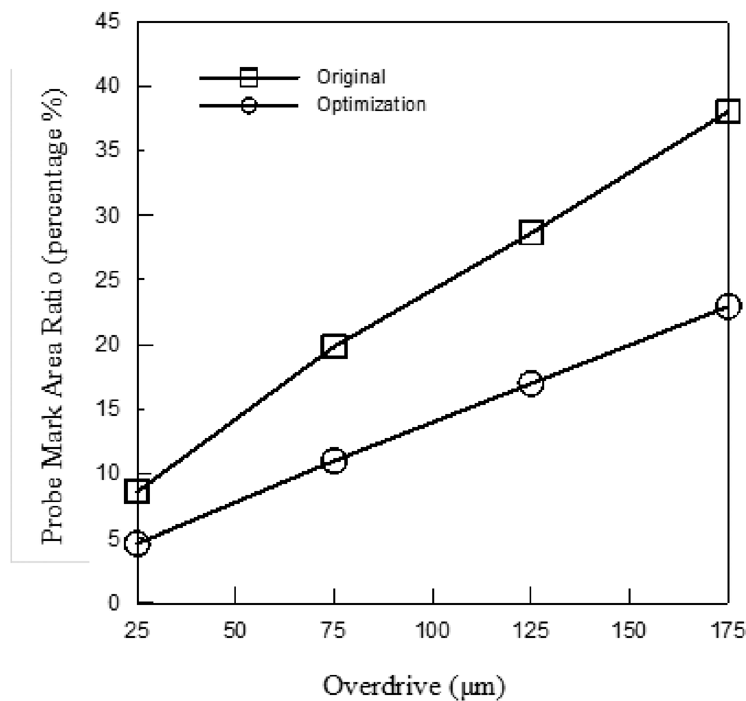

Fig. 16. Relationship between probe mark area ratio and the overdrive under wafer testing of the original and optimization state.

responses of a control factor at different levels. According to the results, the optimal design that leads to the minimum has the combination of (A) probe mid-length at 4100 µm, (B) offset at 1400 µm, (C) rectangle

Table 9. The magnitudes of probe mark area ratio of design optimization under various OD and touchdown times

Touchdown times (N)	OD = 25 μm	OD = 50 μm	OD = 75 μm	OD = 100 μm
1	22.62	29.34	34.26	41.49
2	22.92	31.75	35.19	41.80
3	23.22	31.98	36.11	41.87

Table 10. The magnitudes of bump height of design optimization under various OD and touchdown times

Touchdown times (N)	OD = 25 μm	OD = 50 μm	OD = 75 μm	OD = 100 μm
1	84.23	83.24	83.03	81.74
2	83.93	83.09	82.72	81.42
3	83.64	83.08	82.41	81.25

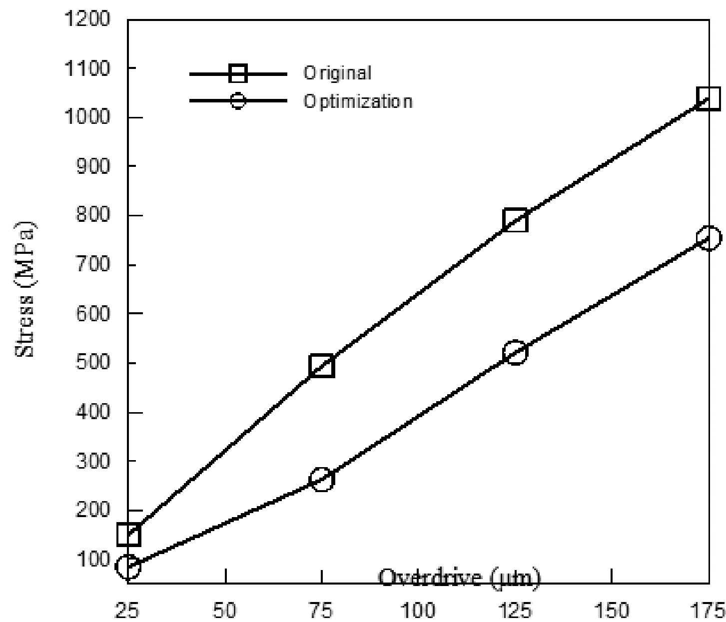

Fig. 17. Relationship between the stress and the overdrive under wafer testing of the original and optimization state.

probe mid-sharp, (D) radius at 4300 μm, and (E) lower die gap at 7.5 μm. This optimal set of parameters leads to a scrub length of 5.3 μm, which is indeed the minimum compared to the results corresponding to the designed experiments in Table 8. For the factors and levels proposed in this study, the probe mid-length (A) has the greatest effect on while needle mid-sharp (C) and the lower die gap (E) are the runners up but with much smaller effects. The probe offset (B), and the needle radius (D) all show insignificant effects on probing mark area ratio. This result has been presented that the probing needle movement is a combination of beam deformation and the design of probing. In addition, the optimization results indicate that a longer mid-length-rectangle cross section and larger lower die gap lead to smaller probing mark area ratio under a constant overdrive distance. On the other hand, it is noted that that the contact surface between the tip and bump is the edge of a flat tip while a smooth surface for a round tips. Form the results, the rectangle probe would therefore lead to a smaller probing mark area ratio than the circle probe. Therefore, it has to be emphasized that the optimization procedure applied in this study characterizes the optimal set and ranking of control factors only for the levels proposed. The argument is further identified by Fig. 14, in which

we show measured probe mark areas ratio with respect to touchdown times for the different overdrive distances. Table 9 shows the magnitudes of probe mark area ratio of design optimization under various OD and touchdown times. It is clear in these figures such that as the touchdown times increase, the probe mark area ratio increase, on the contrary, bump height decrease as the touchdown times increase as shown in Fig. 15. Table 10 shows the magnitudes of bump height of design optimization under various OD and touchdown times. Figures 16 and 17 show that when overdrive is 175 μm, the probe mark area ratio and the maximum von Mises stress are obviously lesser than the original ones by about 47 and 30%, respectively.

4. CONCLUSION

The Taguchi method with the orthogonal array was employed in this paper to obtain an optimal geometrical design of the vertical probing needle based on the minimization of the probing mark and stress inside the needle. The geometrical factors of the needle, including mid-length, offset, mid-sharp, radius and the lower die gap are considered. From the analytical results obtained, the optimal design that leads to the minimum scrub length has the combination of probe mid-sharp with rectangle, probe mid-length at 4100 μm, offset at 1400 μm, mid-sharp at rectangle, radius at 4300 μm and the low die gap at 7.5 μm. For the factors and levels proposed in this study, it has to be noted that the probe mid-length has the greatest effect on the scrub length while probe mid-sharp is rectangle. Furthermore, offset, radius, low die gap, tip diameter all show insignificant effects on the probing mark.

REFERENCES

1. Liu, D.S. and Shih, M.K., “An experimental and numerical investigation into multilayer probe card layout design”, in *I Proc. of IEEE/CPMT-EPM*, pp. 163–171, 2006.
2. Liu, D.S. and Shih, M.K., “Experimental method and FE simulation model for evaluation of wafer probing parameters”, *Microelectronics Journal*, pp. 871–883, 2006.
3. Chang, H.Y., Pan, W.F., Shih, M.K. and Lai, Y.S., “Geometric design for ultra-long needle probe card for digital light processing wafer testing”, *Microelectronics Reliability*, Vol. 50, No. 4, pp. 556–563, 2010.
4. Chang, H.Y., Pan, W.F., Wang, C.C., Taso, Y.C. and Chiang, J.S., “Electrical characterization of micro spring probe card for wafer level testing”, in *Proceedings of 9th International Conference on Electronics Packaging (ICEP)*, Kyoto, Japan, pp. 1–6, 2009.
5. Taber, F.L., “An introduction to area array probing”, in *Proceedings of the International Conference IEEE Southwest Test Workshop*, pp. 277–281, 1998.
6. Beiley, M., Leung, J. and Wong, S.S., “A micro-machined array probe card fabrication process”, *IEEE Transactions on Components, Package and Manufacturing Technology*, Vol. 18, No. 1, pp. 179–183, 1995.
7. Zimmermann, K.F., “Si probe – A new technology for wafer probing”, in *Proceedings of the International Conference IEEE Southwest Test Workshop*, pp. 106–112, 1995.
8. Chang, H.Y., Pan, W.F. and Lin, S.M., “Experimental and theoretical investigation of vertical probe contact behavior of wafer level probing”, *IEEE Transactions on Electronics Packaging Manufacturing*, Vol. 2, No. 4, pp. 710–718, 2012
9. Pardee, B. and Fulton, B., “Using MLO packages to build vertical probe space transformers”, in *Proceedings of the International Conference IEEE Southwest Test Workshop*, pp. 1–25, 2002.
10. *Standard Vertical Probe Card Specifications.* DSL Laboratories, Inc., Fremont, CA [Online]. Available from http://www. dsllab.net/products/vertical.html
11. Primavera, A., “Influence of PCB Parameters on Chip Scale Package Assembly and Reliability (Part I)”, in *Proceedings of SMTA International Conference*, San Jose, CA, 1999.
12. Lau, J.H., “Modeling analysis of 96.5Sn-3.5 lead-free solder joints of wafer level chip scale package on build up microvia pointed circuit board”, *IEEE Transaction on Electronics Packaging Manufacturing*, Vol. 25, pp. 51–58, 2002.

13. Hsiao, H.C., Wen, H.C. and Masaru, N. “A nonlinear growth analysis of integrated device manufacturers’ evolution to the nanotechnology manufacturing outsourcing”, *International Journal of Engineering and Innovative Technology (IJETI)*, Vol. 2, No. 2, pp. 150–162, 2012.
14. Zahn, B.A., “Comprehensive solder fatigue and thermal characterization of a silicon based multi-chip module package utilizing finite element analysis methodologies”, in *Proceedings of 9th International ANSYS Conference*, pp. 1–15, 2000.
15. *Probe Needles for Wafer Sort and Test Applications.* Advanced Probing Systems, Inc. (2002). Available from http://www.advancedprobing.com/
16. Brizmer, V., Kligerman, Y. and Etsion, I., “The effect of contact conditions and material properties on the elasticity terminus of a spherical contact”, *Int. J. Solids Struct.*, Vol. 43, No. 5, pp. 5736–5749, 2006.
17. *Palladium Alloy and Beryllium-Copper Probe Needles.* Advanced Probing Systems, Inc., Boulder, CO [Online]. Available from http://www.advancedprobing.com/